frontiers in Environmental Science

TYPE Original Research
PUBLISHED 08 May 2026
DOI 10.3389/fenvs.2026.1821521

OPEN ACCESS

EDITED BY
Cláudia Pascoal,
University of Minho, Portugal

REVIEWED BY
K. Prasanna,
Birbal Sahni Institute of Palaeosciences (BSIP), India
Xolane Mhlanga,
University of Mpumalanga, South Africa

*CORRESPONDENCE
Peter N. Eze,
peter.eze@uni-potsdam.de

RECEIVED 02 March 2026
REVISED 03 April 2026
ACCEPTED 15 April 2026
PUBLISHED 08 May 2026

CITATION
Dina Ebouel FJ, Bineli Betsi T, Eiche E, Norra S and Eze PN (2026) Decoupling climate and local hydrology in Central Botswana: new insights from carbonate $\delta^{13}C$, $\delta^{18}O$ isotopes, and elemental geochemistry.
Front. Environ. Sci. 14:1821521.
doi: 10.3389/fenvs.2026.1821521

Decoupling climate and local hydrology in Central Botswana: new insights from carbonate $\delta^{13}C$, $\delta^{18}O$ isotopes, and elemental geochemistry

Ferdinand J. Dina Ebouel[1], Thierry Bineli Betsi[2], Elisabeth Eiche[3,4], Stefan Norra[3,5] and Peter N. Eze[1,5]*

[1]Department of Sustainable Natural Resources, Botswana International University of Science and Technology, Palapye, Botswana, [2]Department of Geology and Geological Engineering, Botswana International University of Science and Technology, Palapye, Botswana, [3]Geochemistry and Economic Geology, Institute of Applied Geosciences, Karlsruhe Institute of Technology, Karlsruhe, Germany, [4]Laboratory for Environmental and Raw Materials Analysis (LERA), Institute of Applied Geosciences, Karlsruhe Institute of Technology, Karlsruhe, Germany, [5]Division of Soil Science and Geoecology, Institute of Environmental Science and Geography, University of Potsdam, Potsdam, Germany

Pedogenic carbonates provide valuable archives of past environmental conditions through their elemental and isotopic compositions. This study integrates stable carbon ($\delta^{13}C$) and oxygen ($\delta^{18}O$) isotopes, obtained from carbonate features alongside manganese (Mn) and iron (Fe) concentrations in carbonate features and soil horizons across four pedosedimentary sections (SC01–SC04), to reconstruct vegetation dynamics, climatic stability, and local hydrological variability. Elemental concentrations of Mn and Fe are reported in molar percent (mol%). Soil profiles exhibit low Mn content (0.04%–0.11%), in contrast to higher Fe concentrations (2.68%–7.47%). Carbonate features are systematically depleted in Fe relative to their host matrices (0.42%–3.13%), while Mn is selectively enriched in several nodules, reaching up to 0.22% (Nd07, SC02). Stable isotope data reveal tightly clustered values within each section. $\delta^{13}C$ values range from −3.17‰ to −0.24‰ for nodules, which is consistent with a C4-dominated savannah ecosystem. However, deep-seated pseudomycelia exhibit a distinct $\delta^{13}C$ signature of −6.85‰, interpreted as a biogenic signal from C3 shrub roots in a closed, riparian sub-surface environment rather than a vegetation shift. $\delta^{18}O$ values display a narrow range of −5.52‰ to −3.39‰ across all sections, indicating limited variability in meteoric water composition and evaporative conditions. High Mn/Fe ratios correlate with depleted $\delta^{18}O$ values (≤−5‰), marking periods of increased freshwater input and seasonal waterlogging. Crucially, the decoupling of redox signals in some nodules, characterised by a combined high Mn/Fe ratio with $\delta^{18}O$ enrichment, highlights the occurrence of episodic fluvial pulses and overbank flooding superimposed on a generally semi-arid background. These findings demonstrate that while the regional macro-climate remained stable, local hydrology was highly dynamic, driven by high-frequency fluctuations in river-water influence.

KEYWORDS
fluvial influence, palaeosols, redox processes, semi-arid environments, soil geochemistry, Southern Africa

1 Introduction

Pedogenic carbonate serves as a vital natural pathway for carbon sequestration in arid and semi-arid environments, while also acting as a proxy for past climatic and environmental change (Naorem et al., 2022; Dina Ebouel et al., 2024). These carbonates typically form either through the dissolution and recrystallisation of precursor lithogenic or biogenic minerals such as dolomite or calcite or through the weathering of silicate minerals (Curtis Monger et al., 2015). Both processes play a critical role in the global carbon cycle by facilitating carbon dioxide (CO_2) sequestration through fluvial and marine systems, as well as terrestrial carbon storage within the soil profiles of dryland ecosystems (Lal et al., 2021). While these carbonates are recognised as active pathways for CO_2 sequestration that can be enhanced or degraded by current land use (Raheb et al., 2016; Bughio et al., 2017; An et al., 2019; Liu et al., 2022), they are also frequently identified as the result of long-term accumulation over geological timescales, particularly within palaeosols (Monger, 2014). Consequently, they serve as accurate proxies for palaeoenvironmental and palaeoclimatic reconstruction (Fox et al., 2012; Khormali et al., 2020; Valera-Fernández et al., 2020; Breecker et al., 2025).

The established methodological framework for using pedogenic carbonate as a palaeoenvironmental proxy relies on the origin of the carbon trapped within the mineral lattice, which is primarily derived from root respiration and organic matter decomposition (Zamanian et al., 2016). Consequently, analysing the stable carbon isotope ratios ($\delta^{13}C$) within these carbonates makes it possible to infer the dominant vegetation type (C4 vs. C3 plants) prevailing during their formation (Railsback, 2021; Kirkels et al., 2022). However, the $\delta^{13}C$ signal may also be influenced by the dissolved inorganic carbon (DIC) from which carbonates precipitate, including potential contributions from lithogenic carbonate dissolution (Curtis Monger et al., 2015; Park et al., 2026). In addition, kinetic fractionation during rapid precipitation and post-depositional diagenetic processes may lead to deviations from equilibrium conditions, thereby modifying the primary $\delta^{13}C$ signature (Stoll et al., 2023). As a result, while broad ecological interpretations (e.g., C3 vs. C4 dominance) remain robust, more detailed quantitative reconstructions should be treated with caution (Breecker et al., 2025).

Palaeoclimatic reconstruction is supported by the relationship established between the meteoric water, from which the oxygen present in pedogenic carbonate was derived and the resulting isotopic signature (Cerling, 1984). Thus, the stable isotopic ratio of oxygen in pedogenic carbonate is mainly controlled by the climatic conditions prevailing during mineral precipitation. This is because the fractionation of oxygen isotopes ($^{18}O/^{16}O$) during carbonate precipitation is temperature-dependent, effectively recording the climatic conditions at the time of their formation (Hoefs, 2015). Although seasonal variations and the multiple dissolution-reprecipitation cycles inherent in the development of pedogenic carbonates are often cited as limitations to palaeoenvironmental and palaeoclimatic reconstructions based on stable isotopes (Breecker et al., 2009; Stevenson et al., 2010; Domínguez-Villar et al., 2022), the approach remains demonstrably effective. These processes, while complex, do not negate the capacity of the carbonates to record significant environmental signals, particularly when interpreted within their specific pedosedimentary context (Yang et al., 2012; Zhang et al., 2021; Mohammednoor et al., 2025).

In pedosedimentary environments where active pedogenesis is interrupted by allochthonous deposits, it is often difficult to determine whether these interruptions signify a sustained transition to a humid climate or whether they simply represent isolated large-scale flooding events. However, as established by Sipos et al. (2025), pedogenic carbonates in hydromorphic or fluctuating environments are dynamic archives rather than static minerals. They exist in complex "paragenetic" relationships with other redox-sensitive phases. Mn and Fe in pedogenic carbonates often occur as secondary phases (e.g., oxyhydroxides), and therefore reflect redox dynamics within the soil system rather than strictly syn-depositional conditions. Manganese is reduced and mobilised more rapidly than iron under conditions of increasing anoxia (Otero et al., 2009). Consequently, the relative abundance of these elements in the pedogenic carbonate reflects the specific duration and intensity of the wetting event, allowing transient pulses to be distinguished from prolonged waterlogging.

Pedogenic carbonates play a central role in shaping the pedological landscape of Botswana (Eze, 2022; Dina Ebouel et al., 2025b; Dina Ebouel et al., 2025a). Recently, pedosedimentary sections characterised by significant accumulations of carbonate features have been described along an ephemeral watercourse in the Central District (Dina Ebouel et al. (n.d.), under review). The result demonstrated a pedogenic origin of the carbonate features, in theses sections. Furthermore, mineralogical characterisation identified calcite as the predominant phase. The calcium trapped in these pedogenic carbonates comes mainly from the basaltic bedrock (Eze et al., 2025). However, the high-resolution environmental conditions, particularly the specific vegetative cover and the transient redox dynamics that governed carbonate precipitation, remain poorly constrained. This study aims to reconstruct these palaeoenvironmental conditions, including palaeohydrological fluctuations and redox potentials, by combining stable isotope ($\delta^{13}C$ and $\delta^{18}O$) analyses with the Mn/Fe ratio as a novel redox proxy.

2 Materials and methods

2.1 Study site and sampling strategy

As mentioned above, the study site has already been the subject of other research, particularly with the aim of understanding the formation of the landscape and tracing the origin and processes of calcium ion mobilisation by carbonates (Dina Ebouel et al. (n.d.)). It is in the Central District of Botswana, between 22.34° and 22.42° south latitude and between 26.67° and 26.76° east longitude.

The general environmental setting highlights a relict landscape composed of gently sloping plains interspersed with isolated ravines subject to active erosion, characteristic of the Eastern Hardveld geomorphological unit of Botswana (Atlhopheng et al., 2022). The geological substrate is mainly dominated by the Late Carboniferous to Early Jurassic Karoo Supergroup formations, covered in places by Cenozoic Kalahari Group sands (Smith, 1984). According to the

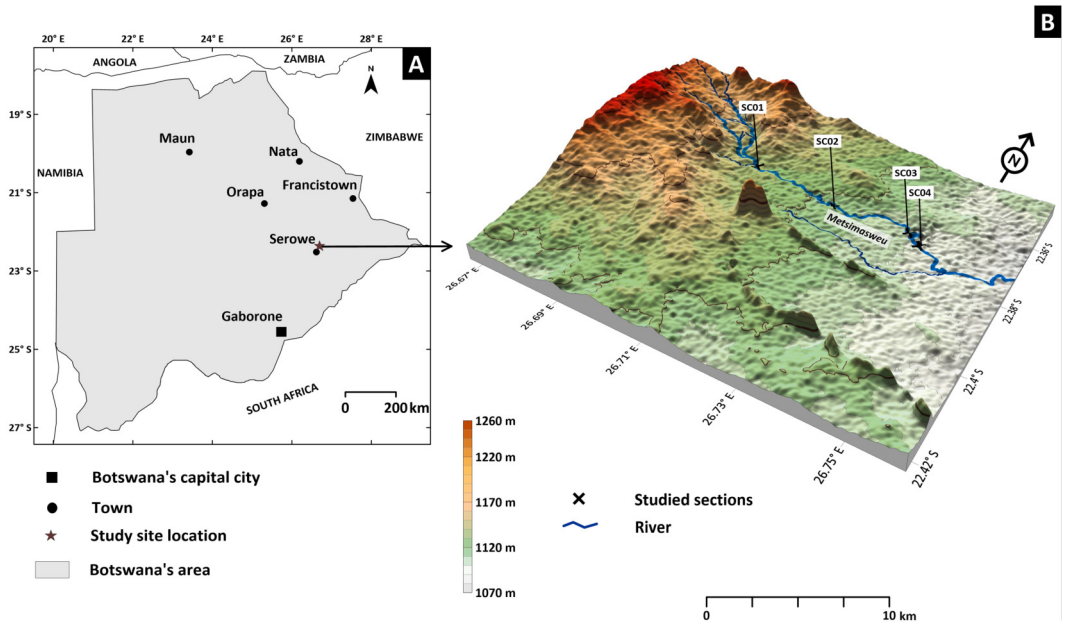

FIGURE 1
(A) localisation of the study area in the map of Botswana; **(B)** 3D topographic model of the study area, showing the river setting and the four selected sections.

lithostratigraphic description of Franchi et al. (2021), the Lower Karoo Supergroup (comprising the Ecca and Beaufort groups) is characterised by a basal sequence of conglomerates and breccias that fines upward into coal-rich mudrocks with organic shales, followed by poorly lithified, grey-to-purple claystones (Beaufort Group). Field observations at the study site reveal a complex stratigraphy where three primary lithologies belonging to the Upper Karoo Supergroup are interbedded. These include alternating mudstones and sandstones from the Lebung Group and basaltic deposits from the Stormberg Lava Group. The Kalahari Group consists of loose aeolian sand containing buried palaeosols rich in carbonate nodules (Franchi et al., 2021).

The local climate is hot and semi-arid (corresponding to BSh type, Köppen–Geiger classification), characterised by long dry periods and a short rainy season from November to March. Rainfall data analysed by Kenabatho (2025) over a 60-year period indicate a mean annual precipitation of approximately 431 mm. However, rainfall is marked by strong interannual variability, with frequent droughts and episodic flooding (Nkemelang et al., 2018; Akinyemi, 2021). The winter season (May to September) is dry and sunny. Daytime temperatures remain warm, whereas nights and early mornings can be cold, with temperatures occasionally reaching 0 °C. Maximum temperatures occur during the summer months and may exceed 45 °C (Batisani and Yarnal, 2010).

Vegetation corresponds to a bush savannah ecosystem, dominated by woody species such as *Acacia, Terminalia*, and *Boscia*, with a diverse herbaceous layer of perennial grasses (Ringrose et al., 1998). This vegetation assemblage reflects a mixed C3–C4 system (Mantlana et al., 2008), in which woody plants are predominantly C3 photosynthetic, whereas the grass layer is largely composed of C4 species (Ellery et al., 1992). Such a vegetation structure is characteristic of semi-arid regions of Botswana (Ellery et al., 1992; Mantlana et al., 2008).

Four pedosedimentary sections were selected along an ephemeral river locally known as Metsimasweu (Figure 1). These sections were selected for their representativity of the local landscape marked by prominent carbonates features in soil. Full description of the sections is given by Dina Ebouel et al. (n.d.). In general, all these sections reflect an alternation between periods of stability, favouring pedogenesis, and periods of instability characterised by fluvial sedimentary deposits resulting from river flooding during wet periods. Thus, the stratigraphy reveals ancient soils (palaeosol) mostly palaeo-Calcisols buried under fluvial sediments, which are themselves covered by poorly developed modern soils, mainly Arenosols or Cambisols. Chemical weathering is generally low, characterised by a low clayeyness and robust chemical weathering index (RW). However, the grain size distribution revealed finer particles towards the downstream sections (SC03 and SC04), reflecting local translocation. The sedimentary layers also show a dominance of angular to sub-angular quartz grains and the presence of opaque fragments, characteristic of accessory minerals in basaltic rocks. This reflects the dominance of local contribution also supported by the presence of basalt and sandstone fragments in soil horizons. The main carbonate features observed are nodules and diffuse powders. Nevertheless, some horizons at the bottom of the sections, generally in contact with or adjacent to the watercourse, often show accumulations in the form of pseudomycelia.

Section (SC01) stands out as the most significant profile in the study. Nodules are present throughout this section, occurring in both the modern soil (Nd01 in the Bk2 horizon; 6.35 wt.% $CaCO_3$) and the buried palaeosols. In the latter, $CaCO_3$ equivalents increase significantly, ranging from 9.39 wt.% in the AB1b horizon (Nd02) to

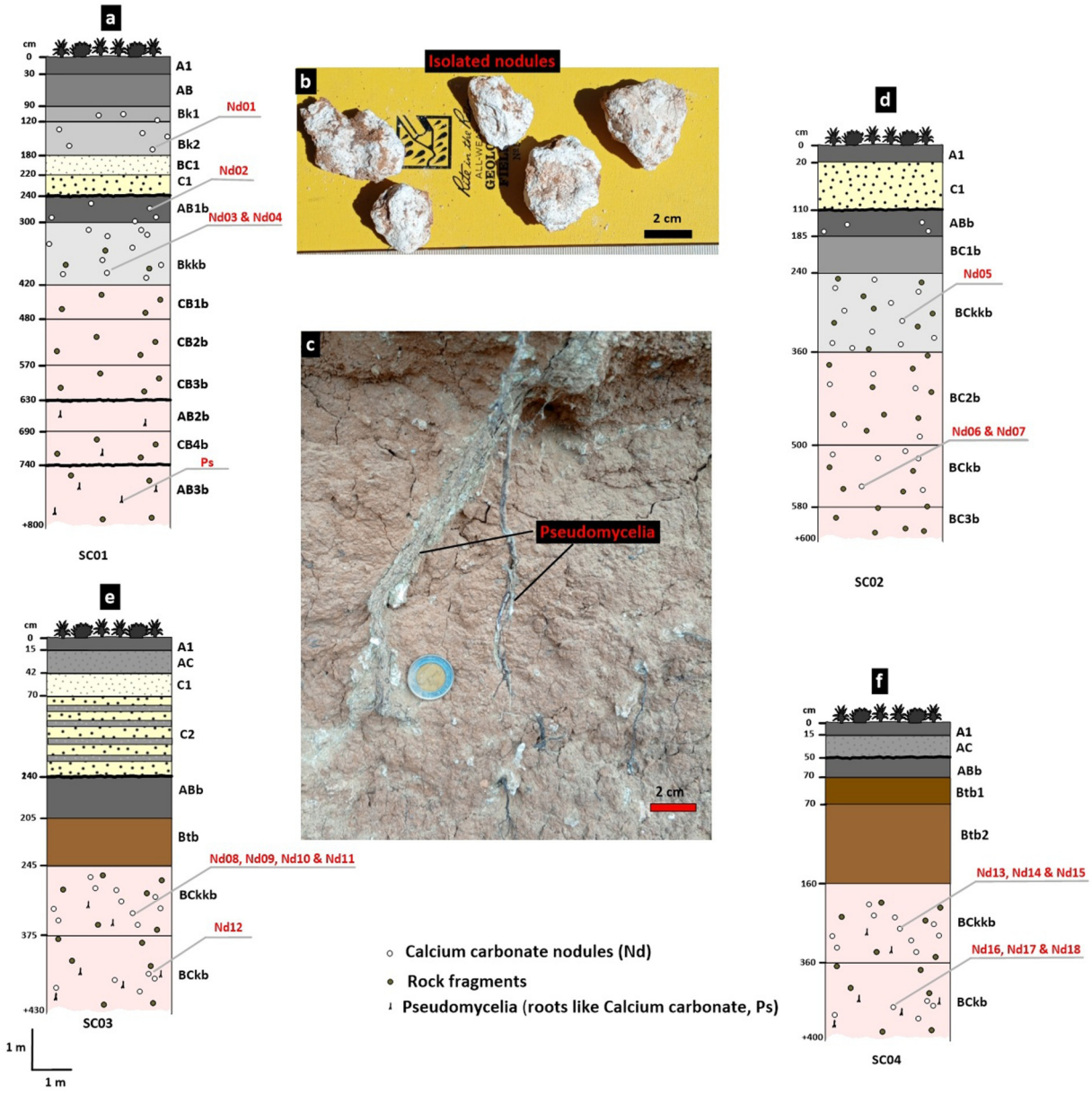

FIGURE 2
(a, d, e, f). Stratigraphy of the four study sections; **(b)** Photograph of calcium carbonate nodules isolated from SC04; and **(c)** Photograph of pseudomycelia calcium carbonate accumulation in SC01.

a peak of 24.61 wt.% in the Bkkb horizons (Nd03, Nd04). Additionally, the base of SC01 is characterised by pseudomycelia (Ps) with a lower carbonate content of 2.18 wt.%. In contrast, carbonate features in the modern soils of SC02, SC03 and SC04 are poorly developed, appearing only in powder form with $CaCO_3$ contents generally below 5 wt.%. Identifiable features are much more prominent in the buried palaeosols of these sections. Specifically, the BCkkb and BCkb horizons across SC02, SC03, and SC04 show a consistent abundance of nodules. The BCkkb horizons consistently exhibit higher concentrations, ranging from 14.24 wt.% in SC02 to 21.09 wt.% in SC04, while the BCkb horizons maintain lower equivalents, fluctuating between 4.00 wt.% and 6.19 wt.%. Full morphological characteristics and physicochemical properties of the four sections are given in Supplementary Table S1.

These carbonate features result primarily from pedogenic processes, with calcite serving as the dominant mineralogical phase. The transition from powdery forms in modern horizons to well-defined nodules in buried layers suggests varying stages of carbonate development and secondary mineral precipitation over time.

Dina Ebouel et al. (n.d.) demonstrated that local basaltic rocks are the dominant source of calcium ions for pedogenic carbonates observed in these sections. This supply involves two distinct pathways: first, the mechanical transport of basaltic fragments

which are reworked into sediments and subsequently incorporated into the soil, where their weathering releases calcium ions to the soil solution that are mobilised by capillary rise and evaporation during the dry season to form secondary carbonates. Second, the *in situ* chemical weathering of the parent material releases calcium ions directly into solution; these ions are then transported by the river and move from the fluvial system into the soil profiles during dry periods, where they are eventually fixed as pedogenic carbonates.

Stratigraphy and locations of carbonate features is presented in Figure 2. Carbonate features (nodules and pseudomycelia) were selectively sampled from horizons displaying significant carbonate accumulation for elemental geochemistry, as well as stable carbon and oxygen isotope analyses. In Section 1 (SC01), five features were collected: nodules Nd01 (Bk2), Nd02 (AB1b), and Nd03–Nd04 (Bkkb), alongside pseudomycelia (Ps) from AB3b. Section 2 (SC02) yielded three nodules, comprising Nd05 (BCkkb) and Nd06–Nd07 (BCkb). Sampling in Section 3 (SC03) included five nodules: Nd08–Nd11 (BCkkb) and Nd12 (BCkb). Finally, six nodules were recovered from Section 4 (SC04), consisting of Nd13–Nd15 (BCkkb) and Nd16–Nd18 (BCkb).

Soil samples were also collected in each horizon of the four soil profiles for elemental geochemical analyses.

2.2 Sample preparation

To ensure the analysis targeted the pedogenic carbonate phase specifically, the samples were cleaned of adhering silicate particles and organic matter. Soil and carbonates samples were then ground into a fine homogeneous powder, using an agate mortar.

2.3 Iron and manganese elemental analysis

Iron and Mn concentrations, originally reported as oxide weight percentages, were determined for all samples (soil and carbonate) using a Bruker AXS S4 Explorer wavelength dispersive X-ray fluorescence spectrometer (WDX), housed at the Laboratory for the Environmental and Raw Materials Analysis (LERA), Institute of Applied Geosciences, Karlsruhe Institute of Technology (KIT), Germany. Analyses were conducted on fused beads. Prior to element quantification, the loss on ignition (LOI) of the pulverised samples was determined by heating them to 950 °C for 3 h and recording the weight difference before and after heating. Fused beads were prepared by mixing the ignited sample powder with a 66.5:33.5 ratio of Li-tetraborate and Li-metaborate (Spectroflux 110, Alfa Aesar) before melting it at 1,000 °C–1,100 °C using a fusion instrument. An Rh X-ray tube (50 keV, 1 kW) was used as the radiation source. Signals were detected using a proportional flow counter (Ar-CH_4 gas) and a scintillation counter. XS-55, LIF2000 and PET were used as analyser crystals. Four certified reference materials, including AGV-1, GXR-2, GXR-5 and Soil 7, were used to verify the accuracy of the produced data. All the uncertainty obtained were below the detection limit.

Mn/Fe ratios in pedogenic carbonates were used as an indirect proxy for redox fluctuations within the soil system, as Sipos et al. (2025) demonstrated that trace Mn and Fe, primarily occurring as secondary oxyhydroxides, are sensitive to hydrological dynamics and redox cycling. To facilitate stoichiometric comparison, bulk geochemical data from soil samples, originally reported as oxide weight percentages (wt.%), were recalculated into elemental molar proportions. For each oxide, the reported weight percentage was divided by its molecular weight to obtain the corresponding oxide molar proportion. This value was then multiplied by the cation stoichiometric coefficient of the oxide (e.g., 2 for Al_2O_3; 1 for CaO) to derive the unnormalised cation molar proportion. Final elemental molar percentages (mol%) were obtained by normalising these values to the total molar sum of all analysed elements (Rollinson and Pease, 2021). This approach ensures that the geochemical signal represents the actual chemical activity and redox-driven availability of these metals in the soil solution at the time of mineral precipitation (Brimhall and Dietrich, 1987; Chadwick et al., 1990).

2.4 Stable isotope analyses

The ratios of stable isotopes of carbon ($^{13}C/^{12}C$) and oxygen ($^{18}O/^{16}O$) in carbonate features were determined at LERA. The samples were analysed for the stable isotope composition of oxygen ($\delta^{18}O$) and carbon ($\delta^{13}C$) by isotope-ratio mass spectrometry (IR-MS) using a Delta V Advantage mass spectrometer (Thermo Fisher Scientific) coupled to an on-line, automated carbonate preparation system (GasBench II; Thermo Fisher Scientific). In this system, the sample vials sealed by rubber septa are flushed with He so that the atmosphere inside the vials is free of CO_2 and O_2, and 103% orthophosphoric acid is added to release CO_2 from the complete dissolution of the ~1 mg carbonate samples over 90 min at 72 °C. Using He as carrier gas, the sample CO_2 then passes a gas-phase chromatograph to separate it from other gases and is injected into the mass spectrometer for analysis (e.g., Clark and Fritz, 1997), in this case in ten pulses of 100 µL each. The results obtained from these ten injections are then averaged to yield the final results.

Calibration was conducted using the NBS19 standard material. Precision is determined by the absolute standard deviation (ASD) of repeated measurements of the Carrara Marble standard material, with an average accuracy of 0.03‰ for $\delta^{13}C$ and of 0.09‰ for $\delta^{18}O$, respectively (n = 150) All results are reported in the δ notation [‰] relative to the V-PDB standard (Supplementary Table S2).

3 Results

3.1 Manganese and iron concentration in the sections

As detailed in Section 2.3, elemental concentrations are reported as molar percentages (mol%). Figure 3 illustrates the vertical variations of Mn and Fe for each study section (numerical values are presented in Supplementary Table S3). Throughout the profiles, Mn occurs primarily as a minor or trace element, ranging from 0.04% to 0.11%, whereas Fe constitutes a major component, with concentrations ranging from 2.68% to 7.47%.

In SC01, the distribution of Mn reveals relative enrichment in horizons Bk1, Bk2, AB1b and Bkkb, where values generally exceed 0.09%. Regarding Fe, a clear stratigraphic distinction emerges: the

10.3389/fenvs.2026.1821521

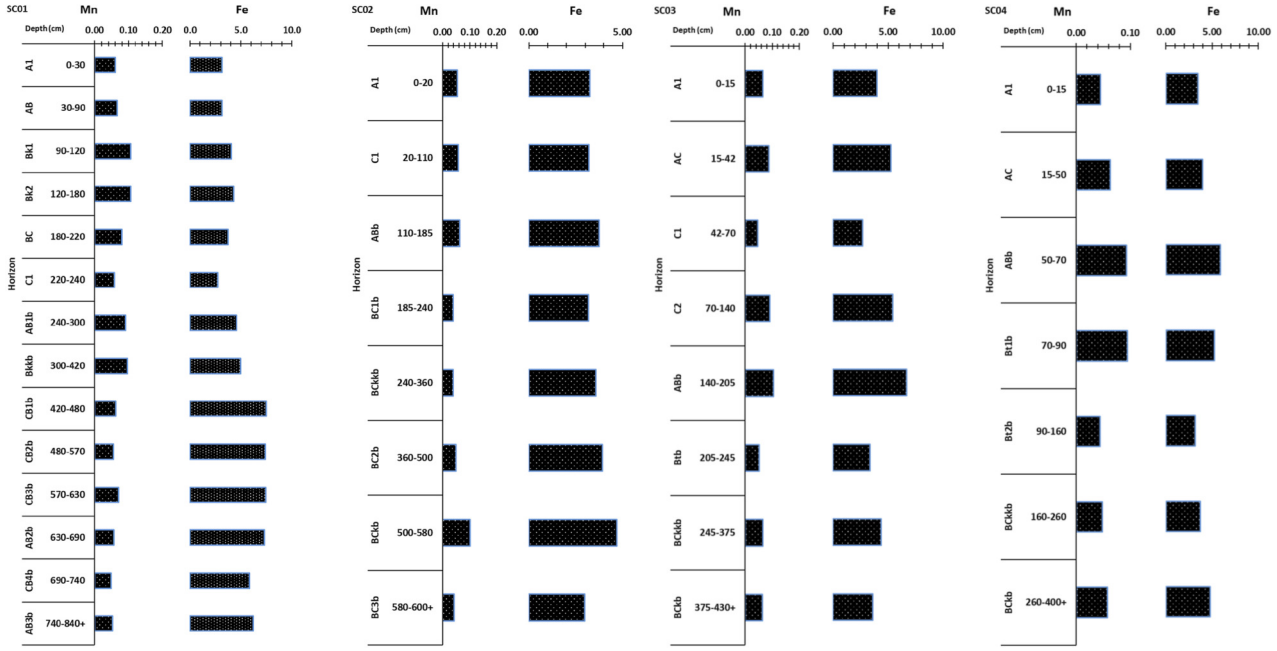

FIGURE 3
Trend of Mn and Fe in the four study sections (SC01, SC02, SC03 and SC04).

TABLE 1 **Manganese and iron contents (mol%) in the selected carbonate features.**

Section	Horizon	Depth (cm)	Sample	Mn	Fe
				(mol%)	
SC01	Bk2	120–180	Nd01	0.06	2.49
	AB1b	240–300	Nd02	0.11	1.16
	Bkkb	300–360	Nd03	0.09	1.22
		360–420	Nd04	0.08	1.53
	AB3b	740–840+	Ps	0.03	3.13
SC02	BCkkb	240–360	Nd05	0.01	0.62
	BCkb	500–540	Nd06	0.16	1.01
		540–580	Nd07	0.22	0.91
SC03	BCkkb	245–285	Nd08	0.10	0.59
		285–305	Nd09	0.05	0.61
		305–345	Nd10	0.04	0.69
		345–375	Nd11	0.05	0.42
	BCkb	375–400	Nd12	0.15	0.69
SC04	BCkkb	160–190	Nd13	0.06	0.86
		190–220	Nd14	0.03	0.62
		220–260	Nd15	0.07	1.04
	BCkb	260–300	Nd16	0.03	0.78
		300–330	Nd17	0.05	0.61
		330–400+	Nd18	0.02	0.90

lower horizons (CB1b to AB3b) exhibit notably higher concentrations (5.86%–7.47%) than the upper sequence (A1 to Bkkb; 2.74%–4.97%).

Sections SC02, SC03 and SC04 display more variable patterns. In SC02, both elements exhibit largely uniform profiles, typically remaining below 0.05% for Mn and 4% for Fe. The BCkb horizon is a notable exception, with higher values of 0.10% Mn and 4.70% Fe. SC03 exhibits a coupled distribution, with peak values for both Mn and Fe occurring in the AC, C2, and ABb horizons, while other horizons remain below 0.05% and 5%, respectively. Similarly, in SC04, both elements follow a twin-peak pattern, with the highest concentrations in the ABb (5.88% for Fe and 0.09% for Mn) and Bt1b (5.23% for Fe and 0.09% for Mn) horizons, while the rest of the profile shows significant depletion.

3.2 Manganese and iron concentration in carbonate features

Table 1 shows the concentrations of Mn and Fe in the carbonate features. The distribution of these elements within the carbonate features contrasts with the patterns observed in the bulk soil profiles. While Fe concentrations are consistently lower than those in the surrounding matrix, Mn concentrations exhibit selective enrichment in several features.

In SC01, most features (Nd01, Nd03, Nd04 and Ps) are depleted in Mn relative to their respective host horizons (Bk2, Bkkb and AB3b). However, Nd02 (0.11%) is an exception, with higher Mn levels than its host, AB1b (0.09%). More pronounced enrichment is observed in SC02, where Nd06 (0.16%) and Nd07 (0.22%) significantly exceed the Mn content

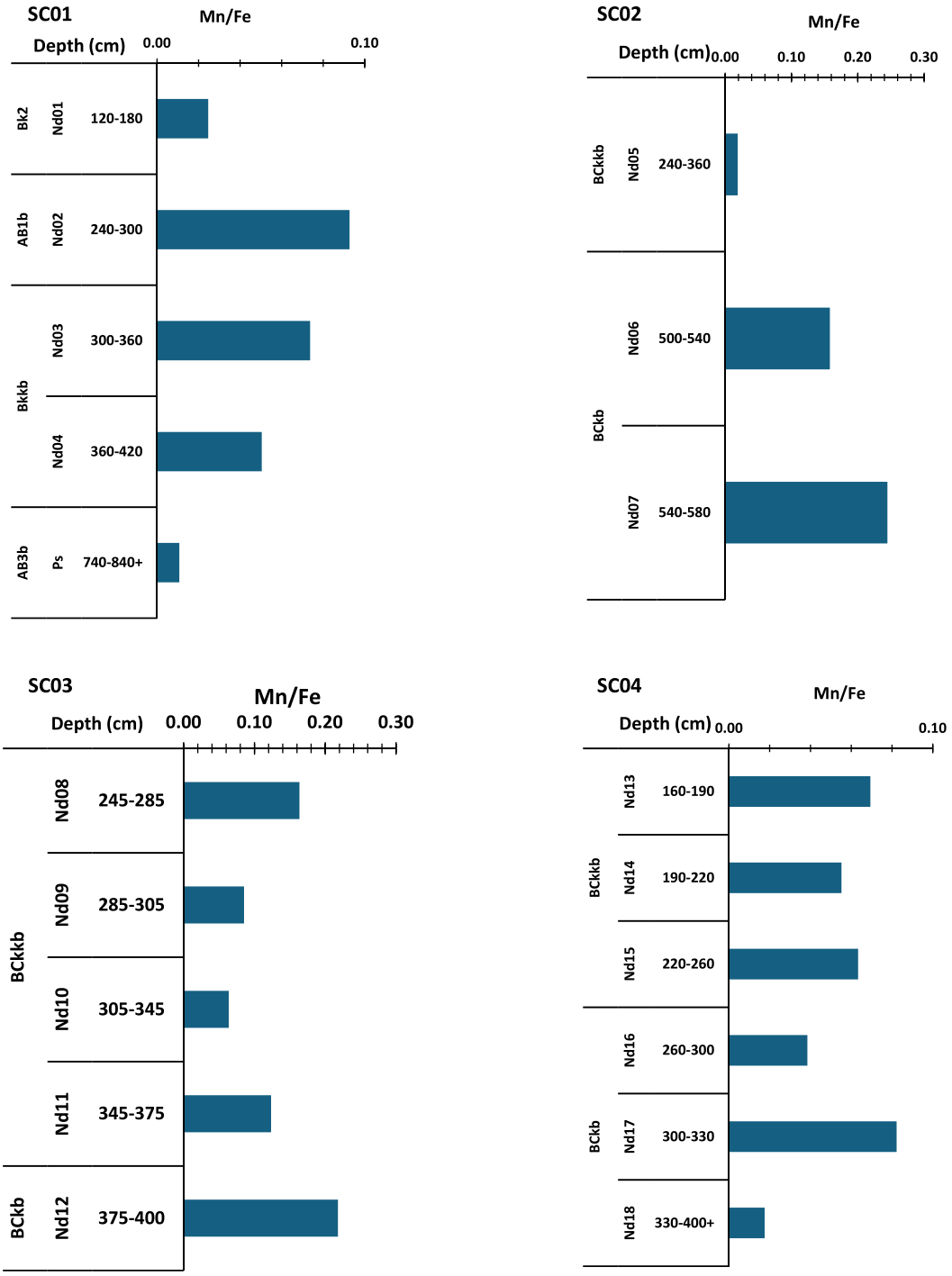

FIGURE 4
Patterns of Mn/Fe ratio of the selected carbonate features.

of their host BCkb (0.09%), though Nd05 (0.01%) remains depleted compared to BCkb (0.04%).

In SC03, Nd08 (0.10%) and Nd12 (0.15%) are similarly enriched relative to their hosts BCkkb (0.06%) and BCkb (0.06%). Nd09 (0.05%), Nd10 (0.04%) and Nd11 (0.05%) in BCkkb follow a contrasting depletion pattern. In SC04, Nd13 (0.06%) and Nd15 (0.07%) have higher Mn content than their host BCkkb (0.04%), while Nd14 (0.03%), Nd16 (0.03%), Nd17 (0.05%) and Nd18 (0.02%) have lower concentrations than their surrounding matrices (BCkb; 0.06%).

The different trends of the ratio Mn/Fe of the selected carbonate features are presented in Figure 4. Overall, features

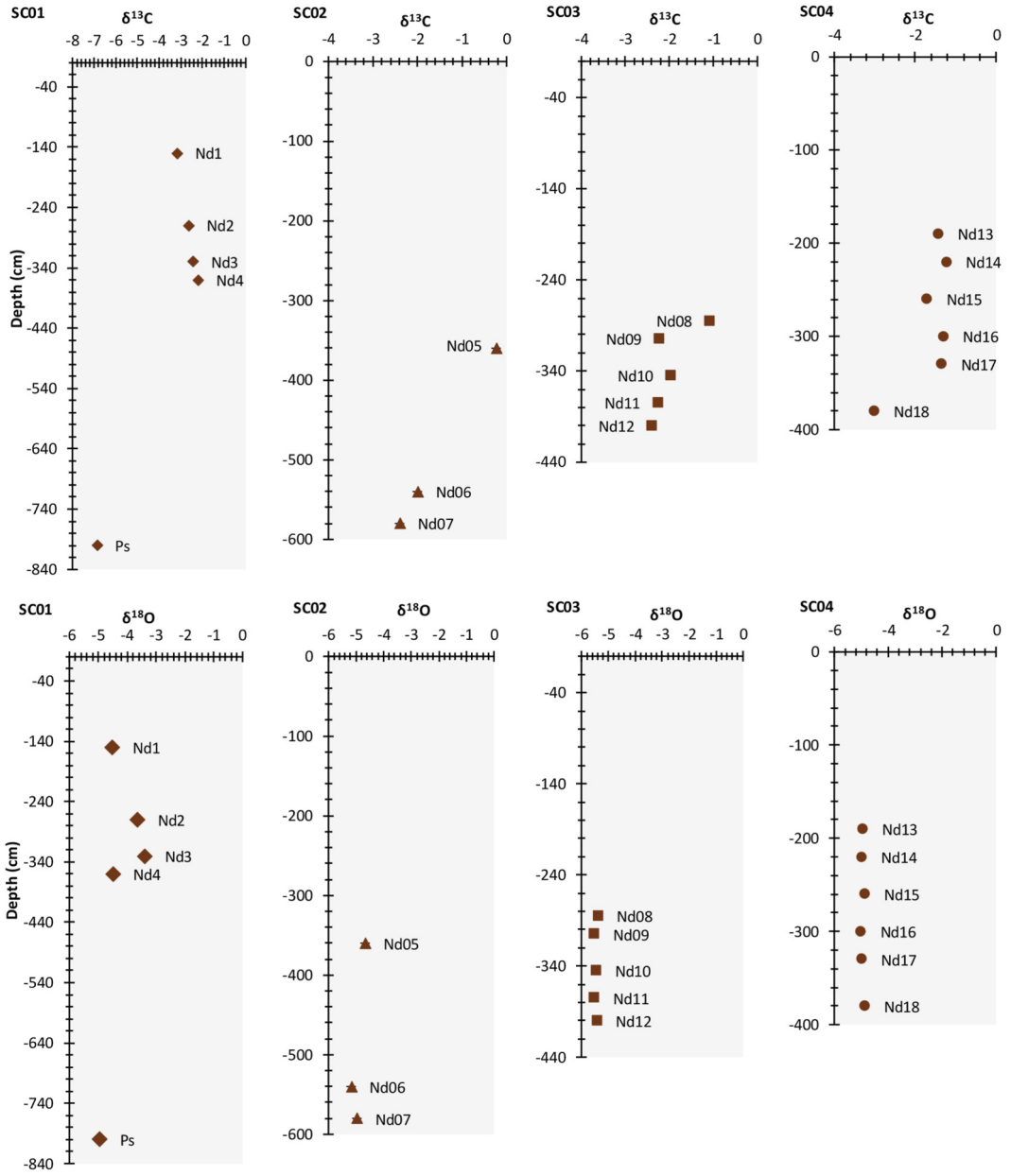

FIGURE 5
Stable carbon and oxygen isotopes of carbonate features.

from sections SC01 (0.01–0.09) and SC04 (0.02–0.08) exhibit lower ratios compared to those from SC02 (0.02–0.24) and SC03 (0.06–0.22). Within SC01, the highest ratio is observed in nodule Nd02 (0.09), followed by Nd03 (0.07), whereas the pseudomycelia (Ps) yield the lowest values (0.01). In SC02, the maximum ratio occurs in Nd07 (0.24), with Nd05 (0.02) representing the minimum for that section. A similar trend is observed in SC03, where Nd12 (0.22) and Nd08 (0.16) display the highest ratios, while Nd10 (0.06) shows the most significant depletion. Finally, in SC04, Nd17 (0.08) reaches the highest ratio, contrasting with Nd18 (0.02) at the base of the section, which records the lowest value.

3.3 Stable isotope of carbon and oxygen in carbonate features

Figure 5 shows the $\delta^{13}C$ and $\delta^{18}O$ values of the carbonate features from the four sections (SC01–SC04), plotted against depth (numerical value are presented in Supplementary Table S2). Across the four sections, $\delta^{13}C$ and $\delta^{18}O$ values define well-structured datasets characterised by relatively narrow ranges and clear clustering within each section. For both isotopic systems, most measurements fall within restricted intervals, with limited dispersion among samples from the same section. Differences between sections are mainly expressed as shifts in the central

value and overall range, rather than as large internal variability. Where present, contrasts between carbonate features are expressed as offsets in isotopic values relative to the dominant clusters.

In SC01, $\delta^{13}C$ values of nodules are tightly grouped between −3.17‰ and −2.19‰. Though within the same range, a slight shift is observed when moving from Nd01 (−3.17‰) in modern soil to Nd02 (−2.63‰) in buried palaeosols. Pseudomycelia at the base of the section is displaying a distinctly lower $\delta^{13}C$ value (−6.85‰), clearly separated from the nodule cluster. The $\delta^{18}O$ values of the nodules in SC01 form a consistent group ranging from −4.49‰ to −3.39‰. Although pseudomycelia have a slightly lower value (−4.94‰), this is not far from the range observed in the nodules.

In SC02, the $\delta^{13}C$ values of the nodules fall within a relatively narrow range between −2.40‰ and −0.24‰. However, there is a slight discrepancy between Nd05 (in BCkkb), exhibiting a $\delta^{13}C$ value of −0.24‰, and the nodules in the horizon below (BCkb), Nd06 and Nd07, with $\delta^{13}C$ values of −2.00 and −2.40‰, respectively. No significant differences were observed in the $\delta^{18}O$ values. They are clustered between −5.17‰ and −4.67‰. In SC03, nodules display compact fields for both stable isotopes. $\delta^{13}C$ values are concentrated between approximately −2.39‰ and −1.08‰. Even though a slight shift toward more negative values is observed with depth. The $\delta^{18}O$ values form a more tightly clustered group, ranging from −5.52‰ to −5.39‰, indicating minimal dispersion within the section.

In SC04, except for a more negative $\delta^{13}C$ observed in Nd18 (−3.00‰), the other nodules have $\delta^{13}C$ values that form a compact group between −1.22‰ and −1.70‰. The $\delta^{18}O$ is characterised by a cluster of values ranging from −5.01‰ to −4.86‰.

4 Discussion

4.1 Vegetation dynamics and stable carbon isotopes in pedogenic carbonates

The relationship between the carbon source of pedogenic carbonates and soil carbon dioxide dynamics has been well established by numerous studies, which show that the carbon incorporated into pedogenic carbonate features is predominantly derived from soil CO_2 produced by plant respiration (Cerling, 1984; Quade et al., 1989; Ryskov et al., 2008; Ning et al., 2025). Consequently, the stable carbon isotope composition ($\delta^{13}C$) of these carbonates is closely linked to the dominant vegetation type (specifically the ratio of C3 to C4 plants) present at the time of precipitation (Cerling and Quade, 1993). In this study, nodules (Nd), which represent the dominant carbonate features, are identified in the upper horizons of section SC01 and throughout the other sections (SC02–SC04). They have $\delta^{13}C$ values ranging from −3.17‰ to −0.24‰. Considering the theoretical enrichment of 14‰–16‰ between soil CO_2 and pedogenic carbonate (Cerling, 1984), the observed values correspond to a soil CO_2 source ranging from −14 to −17‰. Although these values are slightly more negative than a pure C4 biomass signal (average −12‰), they confirm strong C4 dominance. The minor offset suggest that carbonate precipitation occurred in equilibrium with a soil CO_2 reservoir influenced by atmospheric exchange, a condition typical of open-canopy environments with low soil respiration rates (Quade et al., 1989). Moreover, seasonal bias should be considered as pedogenic carbonate accumulation primary occurs during the dry season, reflecting vegetation setting and soil dynamics at that specific time (Fischer-Femal and Bowen, 2021). The similarity between the $\delta^{13}C$ value of Nd01, the nodules observed in modern soil, and the $\delta^{13}C$ values of the numerous nodules in the buried palaeosol in SC01 reveals the dominance of the same type of vegetation over a prolonged period of time. The type of vegetation then remained the same, dominated by C4 plants during the various pedosedimentary cycles.

However, the pseudomycelia (Ps) identified at the bottom of section SC01 (horizon AB3b) show a significantly lower $\delta^{13}C$ value (−7‰). At first glance, this isotopic jump could suggest a transition from vegetation, i.e., a mixed C4-C3 plants to more C3-dominated vegetation (Cerling, 1984). Nevertheless, this interpretation, which would support vegetation different from that currently predominant, is probably erroneous. A distinction in formation dynamics must be made between the different carbonate morphologies identified. While nodules represent cumulative features resulting from long-term pedogenic processes, often averaging environmental signals over millennia (Achyuthan et al., 2010; Diaz et al., 2016; Bayat et al., 2023), pseudomycelia typically reflect an incipient stage of carbonate accumulation. In riparian contexts, these features are frequently linked to high-frequency seasonal fluctuations of the water table (Durand et al., 2010; 2018). Consequently, the pseudomycelia likely capture a more "instantaneous" or modern signal compared to the time-averaged archive preserved within the more recalcitrant nodules. The appearance of pseudomycelia in SC01 is consistent with the immediate proximity of to watercourse. Thus, rather than reflecting a change in vegetation type, this signal seems to reflect current root respiration within this horizon, dominated by shrub roots, which are the only ones to reach this depth. Field observations confirm accumulation along shrub roots (Figure 2). The significant depth of the unit, combined with the hydric influence of the river, would isolate the system from atmospheric CO_2 infiltration, thus allowing the capture of a pure biogenic signal from roots (Quade et al., 1989).

There is, nonetheless, an apparent contradiction between the dominance of herbaceous species, as indicated by the $\delta^{13}C$ values of the nodules, and the bush savannah characterised by the dominance of shrubs (woody species such as *Acacia, Terminalia*, and *Boscia*), as observed in the field and reported in the literature (Ringrose et al., 1998). This discrepancy is consistent with the previously mentioned seasonal bias observed in $\delta^{13}C$ values inherent to carbonate formation (Breecker et al., 2009; Huth et al., 2019). The enriched $\delta^{13}C$ values recorded in the nodules are likely influenced by the timing of carbonate precipitation. As noted by Breecker et al. (2009), pedogenic carbonates in semi-arid environments predominantly form during the dry season via evapotranspiration. During these periods, low soil respiration rates allow for greater atmospheric CO_2 exchange, which further shifts the isotopic composition toward more positive values (Sarangi et al., 2021). On the other hand, the value of −7‰ for deep pseudomycelia reflects the specific signature of C3 shrub roots in a closed environment, thus confirming the coexistence of these two biological forms within a stable savannah structure.

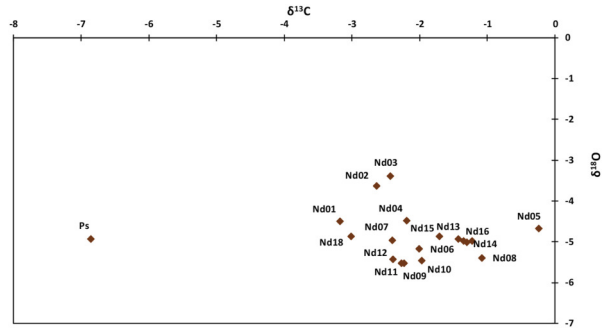

FIGURE 6
Cross-plot of $\delta^{13}C$ and $\delta^{18}O$ for pedogenic carbonate features.

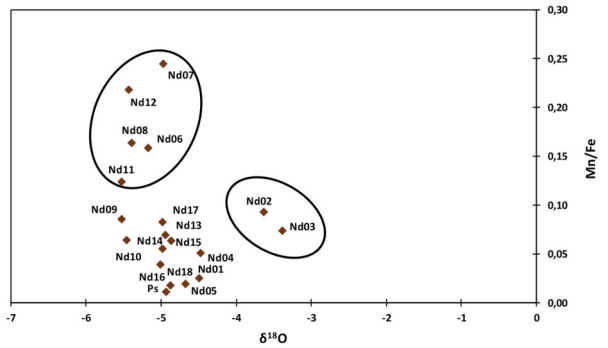

FIGURE 7
Cross-plot of $\delta^{18}O$ and Mn/Fe of pedogenic carbonate features.

4.2 Climate dynamics and stable oxygen isotopes in pedogenic carbonates

The source of oxygen in pedogenic carbonate is meanly related to soil water and therefore, meteoric water (Zamanian et al., 2016). According to Cerling (1984), the $\delta^{18}O$ in pedogenic carbonates records climate because it faithfully tracks the isotopic composition of precipitation, which is itself controlled by temperature and rainfall regime at the time of carbonate formation. In tropical and subtropical regions, the "amount effect" dictates that high precipitation rates lead to a significant decrease in the ^{18}O content of meteoric water (Dansgaard, 1964; Rozanski et al., 1993). This leads to lower $\delta^{18}O$ values in soil carbonates for a given temperature, while dry climates produce enriched ^{18}O values due to low rainfall and intense evaporation (Quade et al., 1989; Fischer-Femal and Bowen, 2021). This enrichment occurs because evaporation preferentially removes the lighter ^{16}O isotope to the atmosphere, leaving residual soil water and the resulting pedogenic carbonates enriched in ^{18}O (Licht et al., 2022). As suggested by our results, the stable oxygen isotopes ($\delta^{18}O$) of the carbonate features in these pedosedimentary sections are clustered around a very narrow range of values from −5.52‰ to −3.39‰. This apparent isotopic homogeneity under comparable hydrological conditions across multiple pedosedimentary sections suggests a period of significant climatic stability. Specifically, it indicates that the isotopic composition of the meteoric water source and the subsequent evaporative enrichment in the soil profile remained relatively constant throughout the period of carbonate precipitation (Cerling, 1984; Quade et al., 1989). This is further highlighted by the cross-plot of $\delta^{13}C$ and $\delta^{18}O$ (Figure 6), which shows a highly concentrated cluster of data points rather than a clear linear trend or several distinct groups. In stable isotope geochemistry, a cluster reflects the absence of significant changes in vegetation type (C4 dominance) or regional water balance (precipitation vs. evaporation). If there had been significant transitions from wet to dry conditions, the samples would likely have been distributed along a "covariation line"; on the contrary, the overlap between modern surface nodules and deeper features reinforces the conclusion that environmental parameters, particularly seasonal aridity and open-canopy savannah structure, remained fundamentally unchanged during the various deposition cycles.

Nevertheless, vertical trends in SC01 highlighted some slight variations in the $\delta^{18}O$ signatures. Nd02 and Nd03 are characterised by relatively high $\delta^{18}O$ values, respectively −3.64‰ and −3.39‰, while Nd01 and Nd04 showed relatively low values, respectively −4.50‰ and −4.48‰. These internal fluctuations likely reflect vertical gradients in soil water evaporation during the time of carbonate precipitation. The enriched (higher) values in Nd02 and Nd03 suggest formation during periods of peak evaporative stress or at shallower depths more exposed to solar radiation. Conversely, the more depleted (lower) values in Nd01 and Nd04 may represent formation during slightly wetter seasons or at depths where soil moisture was better insulated from atmospheric evaporation (Quade et al., 1989; Breecker et al., 2009) The stratigraphic framework established by Dina Ebouel et al. (n.d.) strongly supports this "depth effect" interpretation. According to this stratigraphy, the AB1b horizon containing Nd02 constituted the upper part of the buried palaeosol, likely representing an exposed or near-surface landform prior to the deposition of C1 sediments. The enriched $\delta^{18}O$ signal of Nd03, located in the upper part of the Bkkb horizon, follows this same logic of surface-proximal evaporation. In contrast, the more depleted values in Nd01 (Bk1) and Nd04 (lower Bkkb) reflect carbonate precipitation in deeper accumulation horizons, where the isotopic composition of soil water remains more closely aligned with that of local meteoric water and is less influenced by secondary evaporative enrichment (Cerling and Quade, 1993).

This model of depth-controlled buffering also extends to the pseudomycelia, though their signature is further modified by the specific hydrological dynamics of the riparian zone. Given their proximity to the river channel, these features likely precipitated from groundwater associated with the local watercourse. Their isotopic value represents a balance between the original depleted signature of the river water and subsequent evaporative enrichment at the capillary fringe during periods of water-table recession (Arenas-Abad et al., 2010; Sanz-Montero et al., 2023). This distinguishes the pseudomycelia from the nodules; while the former are controlled by fluctuating groundwater levels near the channel, the latter are primarily influenced by the downward infiltration and evaporation of meteoric waters in the upper soil profile.

4.3 Hydrological conditions and carbonate precipitation

Despite a stable regional climate, Dina Ebouel et al. (n.d.) highlighted localised fluvial changes that interrupted soil development. This dynamic demonstrates the need to analyse variations in local hydrological conditions using Mn/Fe ratios to better understand the specific environment of carbonate formation. Chemical comparisons between pedogenic carbonate features and their host horizons reveal a systematic depletion of iron in the nodules compared to the pedogenic matrix. Conversely, some features (e.g., Nd02, Nd06, Nd07) show significant Mn enrichment. It is important to note that Mn and Fe in pedogenic carbonates are commonly present as secondary oxyhydroxide phases rather than being structurally incorporated into calcite. As a result, Mn/Fe ratios likely integrate both syn- and post-pedogenic redox processes, reflecting fluid circulation, transient saturation, and redox cycling within the soil system (Sipos et al., 2025). This chemical signature aligns with the stratigraphic position of the AB1b horizon (hosting Nd02) in SC01; the overlying C1 deposit indicates a period of fluvial overbank flooding, which would have induced the temporary saturation and reducing conditions necessary to drive this Mn-Fe partitioning.

Figure 7 shows a scatter plot of Mn/Fe ratios versus $\delta^{18}O$ values for carbonate samples. Overall, higher Mn/Fe ratios tend to be associated with more depleted $\delta^{18}O$ values (≤−5‰), whereas samples with less negative $\delta^{18}O$ values cluster at lower Mn/Fe ratios. This likely reflects reducing conditions affecting the soil system, possibly associated with periods of increased moisture and redox fluctuations. Such conditions are consistent with more reducing soil or pore-water environments, in which Mn^{4+} is preferentially reduced and mobilised compared to Fe^{3+}. In contrast, samples characterised by low Mn/Fe ratios likely reflect more oxidising and/or better-drained settings, where Fe remains relatively immobile and Mn availability is limited (Islam and Mostafa, 2023; Sipos et al., 2025).

The dispersion of Mn/Fe ratios at similar $\delta^{18}O$ values indicates that, in addition to the isotopic composition of soil water, local redox heterogeneity and hydrological dynamics (such as fluctuating water tables or episodic saturation) played a major role in controlling trace element signatures. Within this framework, samples Nd02 and Nd03 are distinctive. They combine relatively high Mn/Fe ratios with less negative $\delta^{18}O$ values (around −3.64 to −3.39‰), setting them apart from the main cluster. The $\delta^{18}O$ enrichment suggests precipitation from more evaporated soil waters as mentioned in Section 4.2, and commonly associated with drier conditions. However, their elevated Mn/Fe ratios imply that carbonate recorded episodes of locally reduced conditions, which promoted Mn mobilisation despite an overall evaporative hydrological context (Sipos et al., 2025). Nd02 and Nd03 therefore record a partial decoupling between hydrological and redox signals and are best interpreted as reflecting short-lived reducing events superimposed on a generally dry background climate. These samples likely capture episodic hydrological pulses (e.g., transient saturation following rainfall or perched water tables) rather than sustained wet conditions, highlighting the importance of micro-environmental variability during pedogenic carbonate formation (Driese and Mora, 1993).

The group formed by samples Nd06, Nd07, Nd08, Nd11 and Nd12 exhibits high Mn/Fe ratios that contrast with the stability of their $\delta^{18}O$ signatures. This geochemical trend probably reflects a change related to lithological heritage rather than climatic changes. The local geology consists of alternating basaltic rocks (Mn/Fe ≈ 0.01–0.02), mudstones (Mn/Fe ≈ 0.02) and sandstones (Mn/Fe ≈ 0.03) (Franchi et al., 2021). Furthermore, Dina Ebouel et al. (n.d.) demonstrated that the weathering of these parent materials, individually or in combination, directly influences the development of these pedosedimentary sections. In addition, the absence of oxygen isotopic deviation confirms that these chemical variations occurred under a constant regional climate regime.

In summary, the combination of stable isotopes ($\delta^{13}C$, $\delta^{18}O$) and elemental ratios (Mn/Fe) allows for a reliable reconstruction of a resilient shrub savannah ecosystem. The main strength of this multifaceted approach lies in its ability to dissociate regional climate from local hydrology. While the close clustering of isotopic data indicates long-term regional climate stability and a stable plant structure dominated by C4 plants, Mn/Fe ratios reveal the 'hidden' complexity of the site's fluvial history. Specifically, the ability to correlate Mn enrichment in nodules with stratigraphic evidence of off-channel flooding (e.g., deposit C1) validates the use of the ratio as a high-resolution indicator of transient redox events that isotopic averages might otherwise overlook. However, certain limitations must be acknowledged. The intrinsic "temporal averaging" nature of larger carbonate nodules means that they likely smooth out decades or even centuries of environmental variability, potentially masking short-term ecological changes. Furthermore, the "seasonal bias" of carbonate precipitation, which favours the dry season, means that $\delta^{13}C$ and $\delta^{18}O$ values may disproportionately reflect arid phase conditions rather than the absolute annual mean. While pseudomycelia offer a more "instantaneous" hydrological snapshot, their localised formation along modern root paths and near the riverbed complicates their use as a direct analogue for older, deeper pedosedimentary cycles. Finally, the absence of independent chronological constraints means that a robust temporal framework cannot be established, so interpretations are necessarily process-based rather than time-resolved. Despite these constraints, converging evidence suggests that the study area has maintained a consistent ecological character, punctuated periodically by river pulses, throughout the recorded sections.

5 Conclusion

Overall, the combined analysis of stable isotopes ($\delta^{13}C$ and $\delta^{18}O$) and elemental ratios (Mn/Fe) in pedogenic carbonate features enables the reconstruction of long-term environmental stability and short-lived hydrological disturbances within the study area. The $\delta^{13}C$ values of the carbonate nodules (−3.17‰ to −0.24‰) consistently indicate a resilient, C4-dominated savannah ecosystem. The relatively narrow range of $\delta^{18}O$ values (−5.52‰ to −3.39‰) suggests limited variability in the isotopic composition of soil water; however, this signal should not be interpreted as a direct indicator of regional climatic stability. Instead, it likely reflects a combination of local controls, including evaporation, soil water residence time, and seasonal bias in carbonate precipitation. Minor vertical variations,

particularly in SC01, are therefore more plausibly linked to depth-dependent evaporative processes than to climatic shifts. Meanwhile, Mn/Fe ratios provide valuable insights into redox dynamics and hydrological variability within the soil system, although their interpretation must consider the potential contribution of secondary processes and post-depositional redistribution. Although the time-averaging nature of carbonate precipitation and its seasonal bias may smooth out short-term variability, the convergence of isotopic and elemental evidence suggests that there is a stable ecological framework which is periodically interrupted by river-driven hydrological pulses. Applying this multi-proxy approach to further pedosedimentary sections in different geomorphic settings would enable the evaluation of the regional representativeness of these signals and help to distinguish between local and climate-driven influences. Furthermore, improved chronological constraints would refine the timing and significance of hydrological events.

Data availability statement

The original contributions presented in the study are included in the article/Supplementary Material, further inquiries can be directed to the corresponding author.

Author contributions

FE: Conceptualization, Formal Analysis, Investigation, Methodology, Validation, Visualization, Writing – original draft. TB: Investigation, Methodology, Resources, Supervision, Validation, Writing – review and editing. EE: Data curation, Methodology, Software, Validation, Writing – review and editing. SN: Methodology, Resources, Supervision, Writing – review and editing. PE: Conceptualization, Funding acquisition, Investigation, Methodology, Project administration, Resources, Supervision, Writing – review and editing.

Funding

The author(s) declared that financial support was not received for this work and/or its publication.

Conflict of interest

The author(s) declared that this work was conducted in the absence of any commercial or financial relationships that could be construed as a potential conflict of interest.

Generative AI statement

The author(s) declared that generative AI was not used in the creation of this manuscript.

Any alternative text (alt text) provided alongside figures in this article has been generated by Frontiers with the support of artificial intelligence and reasonable efforts have been made to ensure accuracy, including review by the authors wherever possible. If you identify any issues, please contact us.

Publisher's note

Supplementary material

The Supplementary Material for this article can be found online at: https://www.frontiersin.org/articles/10.3389/fenvs.2026.1821521/full#supplementary-material

References

Achyuthan, H., Flora, O., Braida, M., Shankar, N., and Stenni, B. (2010). Radiocarbon ages of pedogenic carbonate nodules from Coimbatore region, Tamil Nadu. *J. Geol. Soc. India* 75, 791–798. doi:10.1007/s12594-010-0072-2

Akinyemi, F. O. (2021). Vegetation trends, drought severity and land use-land cover change during the growing season in semi-arid contexts. *Remote Sens. (Basel).* 13, 836. doi:10.3390/rs13050836

An, H., Wu, X., Zhang, Y., and Tang, Z. (2019). Effects of land-use change on soil inorganic carbon: a meta-analysis. *Geoderma* 353, 273–282. doi:10.1016/j.geoderma.2019.07.008

Arenas-Abad, C., Vázquez-Urbez, M., Pardo-Tirapu, G., and Sancho-Marcén, C. (2010). "Chapter 3 fluvial and associated carbonate deposits," in *Developments in sedimentology*. Editors A. M. Alonso-Zarza and L. H. Tanner (Oxford, United Kingdom: Elsevier), 133–175. doi:10.1016/S0070-4571(09)06103-2

Atlhopheng, J., Brown Mthanganyika Mapeo, R., and Eckardt, F. D. (2022). "Introduction to the landscapes and landforms of Botswana," in *Landscapes and landforms of Botswana*. Editor F. D. Eckardt (Cham, Switzerland: Springer International Publishing), 1–13. doi:10.1007/978-3-030-86102-5_1

Batisani, N., and Yarnal, B. (2010). Rainfall variability and trends in semi-arid Botswana: implications for climate change adaptation policy. *Appl. Geogr.* 30, 483–489. doi:10.1016/j.apgeog.2009.10.007

Bayat, O., Karimi, A., May, J. H., Fattahi, M., Wiesenberg, G. L. B., and Egli, M. (2023). High-resolution record of stable isotopes in soil carbonates reveals environmental dynamics in an arid region (central Iran) during the last 32 ka. *Front. Earth Sci. (Lausanne).* 11, 1154544. doi:10.3389/feart.2023.1154544

Breecker, D. O., Sharp, Z. D., and McFadden, L. D. (2009). Seasonal bias in the formation and stable isotopic composition of pedogenic carbonate in modern soils from central New Mexico, USA. *Bull. Geol. Soc. Am.* 121, 630–640. doi:10.1130/B26413.1

Breecker, D. O., Michel, L. A., Rasmussen, C., and Tabor, N. J. (2025). "A biogeochemical perspective on pedogenesis from soils to paleosols," in *Treatise on geochemistry*. Editors A. Anbar and D. Weis Third edition (Oxford, United Kingdom: Elsevier), 353–409. doi:10.1016/B978-0-323-99762-1.00094-2

Brimhall, G. H., and Dietrich, W. E. (1987). Constitutive mass balance relations between chemical composition, volume, density, porosity, and strain in metasomatic hydrochemical systems: results on weathering and pedogenesis. *Geochim. Cosmochim. Acta* 51, 567–587. doi:10.1016/0016-7037(87)90070-6

Bughio, M. A., Wang, P., Meng, F., Chen, Q., Li, J., and Shaikh, T. A. (2017). Neoformation of pedogenic carbonate and conservation of lithogenic carbonate by farming practices and their contribution to carbon sequestration in soil. *Z Pflanzenernaehr Bodenkd.* 180, 454–463. doi:10.1002/jpln.201500650

Cerling, T. E. (1984). The stable isotopic composition of modern soil carbonate and its relationship to climate. *Earth Planet. Sci. Lett.* 71, 229–240. doi:10.1016/0012-821X(84)90089-X

Cerling, T. E., and Quade, J. (1993). "Stable carbon and oxygen isotopes in soil carbonates," in *Climate change in Continental isotopic records*. Washington, DC: AGU, 217–231. doi:10.1029/GM078p0217

Chadwick, O. A., Brimhall, G. H., and Hendricks, D. M. (1990). From a black to a gray box — a mass balance interpretation of pedogenesis. *Geomorphol.* 3, 369–390. doi:10.1016/0169-555X(90)90012-F

Clark, I., and Fritz, P. (1997). *Environmental isotopes in hydrogeology*. 1st Edn. Boca Raton, FL: CRC Press. Available online at: https://doi.org/10.1201/9781482242911 (Accessed April 1, 2026).

Curtis Monger, H., Kraimer, R. A., Khresat, S., Cole, D. R., Wang, X., and Wang, J. (2015). Sequestration of inorganic carbon in soil and groundwater. *Geology* 43, 375–378. doi:10.1130/G36449.1

Dansgaard, W. (1964). Stable isotopes in precipitation. *Tellus* 16, 436–468. doi:10.1111/j.2153-3490.1964.tb00181.x

Diaz, N., King, G. E., Valla, P. G., Herman, F., and Verrecchia, E. P. (2016). Pedogenic carbonate nodules as soil time archives: challenges and investigations related to OSL dating. *Quat. Geochronol.* 36, 120–133. doi:10.1016/j.quageo.2016.08.008

Dina Ebouel, F. J., Betsi, T. B., and Eze, P. N. (2024). Soil inorganic carbon: a review of global research trends, analytical techniques, ecosystem functions and critical knowledge gaps. *Catena (Amst)* 242, 108112. doi:10.1016/j.catena.2024.108112

Dina Ebouel, F. J., Kono Ebede, C. G., Bineli Betsi, T., and Eze, P. N. (2025a). Distribution and potential of rare earth elements fingerprinting as tracers for carbonate sources in soils developed on contrasting parent materials. *Geoderma Reg.* 43, e01009. doi:10.1016/j.geodrs.2025.e01009

Dina Ebouel, F. J., Molwalefhe, L. N., Betsi, T. B., and Eze, P. N. (2025b). A multi-proxy pedosedimentary insight into calcium origin, sediment provenance, and depositional environments in a NW Botswana landform. *Earth Syst. Environ.* 9, 1937–1957. doi:10.1007/s41748-025-00724-w

Dina Ebouel, F. J., Bineli Betsi, T., Eiche, E., and Norra, S. ((n.d.)). Pedogenic and sedimentary controls on secondary carbonate accumulation in semi-2 arid fluvial landscape. *Central Botswana*. doi:10.2139/ssrn.6330138

Domínguez-Villar, D., Bensa, A., Švob, M., and Krklec, K. (2022). Causes and implications of the seasonal dissolution and precipitation of pedogenic carbonates in soils of karst regions – a thermodynamic model approach. *Geoderma* 423, 115962. doi:10.1016/J.GEODERMA.2022.115962

Driese, S. G., and Mora, C. I. (1993). Physico-chemical environment of pedogenic carbonate formation in Devonian vertic palaeosols, central Appalachians, USA. *Sedimentology* 40, 199–216. doi:10.1111/j.1365-3091.1993.tb01761.x

Durand, N., Monger, H. C., and Canti, M. G. (2010). "9 - calcium carbonate features," in *Interpretation of micromorphological features of soils and regoliths*. Editors G. Stoops, V. Marcelino, and F. Mees (Amsterdam, Netherlands: Elsevier), 149–194. doi:10.1016/B978-0-444-53156-8.00009-X

Durand, N., Monger, H. C., Canti, M. G., and Verrecchia, E. P. (2018). "Calcium carbonate features," in *Interpretation of micromorphological features of soils and regoliths* (Amsterdam, Netherlands: Elsevier), 205–258. doi:10.1016/b978-0-444-63522-8.00009-7

Ellery, K., Ellery, W. N., and Verhagen, B.Th. (1992). The distribution of C3 and C4 plants in a successional sequence in the okavango Delta. *South Afr. J. Bot.* 58, 400–402. doi:10.1016/S0254-6299(16)30829-8

Eze, P. N. (2022). "Soil development in the Eastern hardveld," in *Landscapes and landforms of Botswana*. Editor F. D. Eckardt (Cham, Switzerland: Springer International Publishing), 327–344. doi:10.1007/978-3-030-86102-5_19

Eze, P. N., Dina Ebouel, F. J., Nkonga, I., Musiol, A., Schleicher, A. M., and Günter, C. (2025). Weathering intensity and trace elements (Ni, Sr, Zn, and Cr) distribution in Vertisols developed on basalt in a semiarid environment: agronomic implications. *Front. Soil Sci.* 5. doi:10.3389/fsoil.2025.1530962

Fischer-Femal, B. J., and Bowen, G. J. (2021). Coupled carbon and oxygen isotope model for pedogenic carbonates. *Geochim. Cosmochim. Acta* 294, 126–144. doi:10.1016/j.gca.2020.10.022

Fox, D. L., Honey, J. G., Martin, R. A., and Peláez-Campomanes, P. (2012). Pedogenic carbonate stable isotope record of environmental change during the Neogene in the southern great plains, southwest Kansas, USA: oxygen isotopes and paleoclimate during the evolution of C4-dominated grasslands. *Bull. Geol. Soc. Am.* 124, 431–443. doi:10.1130/B30402.1

Franchi, F., Kelepile, T., Di Capua, A., De Wit, M. C. J., Kemiso, O., Lasarwe, R., et al. (2021). Lithostratigraphy, sedimentary petrography and geochemistry of the upper karoo supergroup in the Central Kalahari Karoo Sub-Basin, Botswana. *J. Afr. Earth Sci.* 173, 104025. doi:10.1016/j.jafrearsci.2020.104025

Hoefs, J. (2015). "Isotope fractionation processes of selected elements," in *Stable isotope geochemistry*. Editor J. Hoefs (Cham, Switzerland: Springer International Publishing), 47–190. doi:10.1007/978-3-319-19716-6_2

Huth, T. E., Cerling, T. E., Marchetti, D. W., Bowling, D. R., Ellwein, A. L., and Passey, B. H. (2019). Seasonal bias in soil carbonate formation and its implications for interpreting high-resolution paleoarchives: evidence from Southern Utah. *J. Geophys. Res. Biogeosci.* 124, 616–632. doi:10.1029/2018JG004496

Islam, Md. S., and Mostafa, M. G. (2023). Occurrence, source, and mobilization of iron, manganese, and arsenic pollution in shallow aquifer. *Geofluids* 2023, 1–19. doi:10.1155/2023/6628095

Kenabatho, P. K. (2025). Innovative trend analysis of long-term spatial-temporal rainfall patterns over Botswana: implications for water resources management. *J. Hydrol. Reg. Stud.* 58, 102217. doi:10.1016/j.ejrh.2025.102217

Khormali, F., Shahriari, A., Ghafarpour, A., Kehl, M., Lehndorff, E., and Frechen, M. (2020). Pedogenic carbonates archive modern and past precipitation change – a transect study from soils and loess-paleosol sequences from northern Iran. *Quat. Int.* 552, 79–90. doi:10.1016/j.quaint.2019.12.011

Kirkels, F. M. S. A., De Boer, H. J., Concha Hernández, P., Martes, C. R. T., Van Der Meer, M. T. J., Basu, S., et al. (2022). Carbon isotopic ratios of modern C3 and C4 vegetation on the Indian peninsula and changes along the plant-soil-river continuum - implications for vegetation reconstructions. *Biogeosciences* 19, 4107–4127. doi:10.5194/bg-19-4107-2022

Lal, R., Monger, C., Nave, L., and Smith, P. (2021). The role of soil in regulation of climate. *Philosophical Trans. R. Soc. B Biol. Sci.* 376, 20210084. doi:10.1098/rstb.2021.0084

Licht, A., Kelson, J., Bergel, S., Schauer, A., Petersen, S. V., Capirala, A., et al. (2022). Dynamics of pedogenic carbonate growth in the tropical domain of Myanmar. *Geochem. Geophys. Geosystems* 23, e2021GC009929. doi:10.1029/2021GC009929

Liu, J., Wu, P., Zhao, Z., and Gao, Y. (2022). Afforestation on cropland promotes pedogenic inorganic carbon accumulation in deep soil layers on the Chinese loess plateau. *Plant Soil* 478, 597–612. doi:10.1007/s11104-022-05494-2

Mantlana, K. B., Arneth, A., Veenendaal, E. M., Wohland, P., Wolski, P., Kolle, O., et al. (2008). Photosynthetic properties of C4 plants growing in an African savanna/wetland mosaic. *J. Exp. Bot.* 59, 3941–3952. doi:10.1093/jxb/ern237

Mohammednoor, M., Bibi, F., Struck, U., Eisawi, A., and Bussert, R. (2025). Pleistocene pedogenic carbonates from alluvial paleosols in eastern Sudan reveal a semi-arid and seasonal climate, similar to today. *Catena (Amst).* 248, 108583. doi:10.1016/j.catena.2024.108583

Monger, H. C. (2014). "Soils as generators and sinks of inorganic carbon in geologic time," in *Soil carbon* (Cham, Switzerland: Springer International Publishing), 27–36. doi:10.1007/978-3-319-04084-4_3

Naorem, A., Jayaraman, S., Dalal, R. C., Patra, A., Rao, C. S., and Lal, R. (2022). Soil inorganic carbon as a potential sink in carbon storage in dryland soils—A review. *Agric. (Switzerland)* 12, 1256. doi:10.3390/agriculture12081256

Ning, M., Luo, J., Liang, Z., Huang, P., Xing, C., and Shen, B. (2025). Pedogenic carbonates in deep time: characteristics, geological significance, and co-evolution with plant terrestrialization. *Earth. Sci. Rev.* 271, 105314. doi:10.1016/j.earscirev.2025.105314

Nkemelang, T., New, M., and Zaroug, M. (2018). Temperature and precipitation extremes under current, 1.5 °C and 2.0 °C global warming above pre-industrial levels over Botswana, and implications for climate change vulnerability. *Environ. Res. Lett.* 13, 065016. doi:10.1088/1748-9326/aac2f8

Otero, X. L., Ferreira, T. O., Huerta-Díaz, M. A., Partiti, C. S. M., Souza, V., Vidal-Torrado, P., et al. (2009). Geochemistry of iron and manganese in soils and sediments of a mangrove system, Island of Pai Matos (Cananeia — SP, Brazil). *Geoderma* 148, 318–335. doi:10.1016/j.geoderma.2008.10.016

Park, S.-W., Baek, N., Shin, E.-S., Seo, B.-S., Lee, S.-I., Lee, K.-S., et al. (2026). Substitution of lithogenic with pedogenic soil carbonates in Korean coastal rice paddy under desalinization: evidences from δ13C. *Agric. Ecosyst. Environ.* 396, 109993. doi:10.1016/j.agee.2025.109993

Quade, J., Cerling, T. E., and Bowman, J. R. (1989). Systematic variations in the carbon and oxygen isotopic composition of pedogenic carbonate along elevation transects in the southern Great Basin, United States. *GSA Bull.* 101, 464–475. doi:10.1130/0016-7606(1989)101<0464:SVITCA>2.3.CO;2

Raheb, A., Heidari, A., and Mahmoodi, S. (2016). Storage of organic and inorganic carbon in arid-semihumid soils: a case study of the rangelands of northwestern Iran. *Soil Sci.* 181, 473–486. doi:10.1097/SS.0000000000000183

Railsback, L. B. (2021). Pedogenic carbonate nodules from a forested region of humid climate in central Tennessee, USA, and their implications for interpretation of C3-C4 relationships and seasonality of meteoric precipitation from carbon isotope (δ13C) data. *Catena (Amst)* 200, 105169. doi:10.1016/j.catena.2021.105169

Ringrose, S., Matheson, W., and Vanderpost, C. (1998). Analysis of soil organic carbon and vegetation cover trends along the Botswana Kalahari Transect. *J. Arid Environ.* 38, 379–396. doi:10.1006/jare.1997.0344

Rollinson, H., and Pease, V. (Editors) (2021). "Using major element data," in *Using geochemical data: to understand geological processes* (Cambridge:

United Kingdom, Cambridge University Press), 49–95. doi:10.1017/9781108777834.006

Rozanski, K., Araguás-Araguás, L., and Gonfiantini, R. (1993). "Isotopic patterns in modern global precipitation," in *Climate change in Continental isotopic records* (Washington, DC: AGU), 1–36. doi:10.1029/GM078p0001

Ryskov, Y. G., Velichko, A. A., Nikolaev, V. I., Oleinik, S. A., Timireva, S. N., Nechaev, V. P., et al. (2008). Reconstruction of the paleotemperature and precipitation in the Pleistocene according to the isotope composition of humus and carbonates in loess on the Russian Plain. *Eurasian Soil Sci.* 41, 937–945. doi:10.1134/S1064229308090044

Sanz-Montero, M. E., del Buey, P., Cabestrero, Ó., and Sánchez-Román, M. (2023). Isotopic signatures of microbial Mg-Carbonates deposited in an ephemeral Hyperalkaline Lake (Central Spain): paleoenvironmental implications. *Minerals* 13, 617. doi:10.3390/min13050617

Sarangi, V., Agrawal, S., and Sanyal, P. (2021). The disparity in the abundance of C4 plants estimated using the carbon isotopic composition of paleosol components. *Palaeogeogr. Palaeoclimatol. Palaeoecol.* 561, 110068. doi:10.1016/j.palaeo.2020.110068

Sipos, P., Kovács, I., Tóth, A., Németh, P., and Demény, A. (2025). Paragenetic relationship between ferromanganese and calcareous nodules in a hydromorphic toposequence. *Geoderma* 454, 117179. doi:10.1016/j.geoderma.2025.117179

Smith, A. R. (1984). The lithostratigraphy of the Karoo supergroup in Botswana. *Geol. Mag.* 123, 710–711. doi:10.1017/S0016756800024328

Stevenson, B. A., Kelly, E. F., McDonald, E. V., Busacca, A. J., and Welker, J. M. (2010). Oxygen isotope ratios in Holocene carbonates across a climatic gradient, eastern Washington State, USA: evidence for seasonal effects on pedogenic mineral isotopic composition. *Holocene* 20, 575–583. doi:10.1177/0959683609356588

Stoll, H. M., Day, C., Lechleitner, F., Kost, O., Endres, L., Sliwinski, J., et al. (2023). Distinguishing the combined vegetation and soil component of δ13C variation in speleothem records from subsequent degassing and prior calcite precipitation effects. *Clim. Past* 19, 2423–2444. doi:10.5194/cp-19-2423-2023

Valera-Fernández, D., Cabadas-Báez, H., Solleiro-Rebolledo, E., Landa-Arreguín, F. J., and Sedov, S. (2020). Pedogenic carbonate crusts (calcretes) in karstic landscapes as archives for paleoenvironmental reconstructions – a case study from Yucatan Peninsula, Mexico. *Catena (Amst)* 194, 104635. doi:10.1016/j.catena.2020.104635

Yang, S., Ding, Z., Wang, X., Tang, Z., and Gu, Z. (2012). Negative δ 18O-δ 13C relationship of pedogenic carbonate from northern China indicates a strong response of C 3/C 4 biomass to the seasonality of Asian monsoon precipitation. *Palaeogeogr. Palaeoclimatol. Palaeoecol.* 317–318, 32–40. doi:10.1016/j.palaeo.2011.12.007

Zamanian, K., Pustovoytov, K., and Kuzyakov, Y. (2016). Pedogenic carbonates: forms and formation processes. *Earth. Sci. Rev.* 157, 1–17. doi:10.1016/j.earscirev.2016.03.003

Zhang, D., Beverly, E. J., Levin, N. E., Vidal, E., Matia, Y., and Feakins, S. J. (2021). Carbon isotopic composition of plant waxes, bulk organics and carbonates from soils of the Serengeti grasslands. *Geochim. Cosmochim. Acta* 311, 316–331. doi:10.1016/j.gca.2021.07.005